Stress Analysis of FGM Rotating Disk Subjected to Mechanical and Thermal Loads In Aircraft Gas Turbine Engine

B. Shahriari*, M. Safari

Department of Mechanical Engineering, Malek Ashtar University of Technology, Isfahan, Iran

ABSTRACT

Pursuant to the high usage of rotating the disk in aircraft gas turbine engine, turbo pumps in oil and gas industries, steam and gas turbines in power plants, marine gas turbine and other industrial rotary machines designing and getting under the mechanical and thermal loading casued this design and analysis to be as a special significance. These disks are subjected to mechanical and thermal loads. In this article, four methods, variable material properties (VMP), Galerkin, Runge-Kutta with two different rules compute the amount of displacement, stress, and strain of a rotary disk, which has been applied from a functionally graded material (FGM). The problem in dissimilar states of loading and temperature dependence and independence of the properties has been resolved. Disk properties with the specified function of radius change. Mechanical loading conditions result from the centrifugal disk and blades mounted on it and the effects of shaft pressure and thermal stress caused by temperature difference in the shaft. The results acquired through every four methods are closed together and can be applied to analyse the problems of this type. Combining all loads, the most radial stresses and environmental stresses respectively obtained in the center of the inner and outer radius and inner radius of the disk. Through applying the results can get most optimal design of the (FGM) disk.

1. Introduction

In recent years, with the increasing growth of different industries and improvement of industrial machines and also development of strong engines in aerospace industries, turbines, reactors, and other machines, more materials with higher thermal resistance are required. Functional scaled materials that would have a proper mechanical strength under high temperatures against imposed stresses are nowadays a proper matter to be applied in above mentioned activities. The main purpose of designing and production of structures is to decrease weight, reduce costs, boost the strength, and to have a proper response against imposed stresses. Regarding FGM matter for each structure, all of the above advantages can be achieved approximately. In order to design each structure, knowledge about their strength response in different loading conditions is required–Consequently, this problem must be analyzed under dissimilar structure analysis such as stress and strain analysis in different loadings. Rotary disk in turbine engine of air gasses is under strict thermal gradients and strict mechanical loadings as some examples of eccentricity forces. Designing this disk by applying FGM materials can lead to generating a disk with high structure operating. In this way, the exact analysis of stress and strain of these elements can lead to a proper design for them.

Sahni and Sahni proposed an analytical solution to compute stresses made of functionally graded materials subjected to the variable thickness and external pressure. The Poisson ratio is taken as constant [1]. B. Arnab worked analysis of thermoelastic filed in a thin circular functionally graded material disk with a concentric hole subjected to thermal loads. The analysis of the results reveals that the thermoelastic characteristics of an FGM disk is substantially dependent on material distribution as well as difference of temperatures at the inner and outer surfaces of the disk [2]. Bayat presented the magneto-thermo-mechanical response of a functionally graded magnetoelastic material (FGMM) annular variable-thickness rotating disk. It can be observed that despite the radial stress in a mounted FGM disk subjected to mechanical load only where it is usually tensile, the radial stress as

* Corresponding author Tel.: +98-9131254280; Fax: +98-31-45227136
E-mail address: shahriari@mut-es.ac.ir

a result of magneto-thermal load in a mounted FGMM disk can be both tensile and compressive type [3]. Dai inspected a way to find the displacement and stress fields in a functionally graded material hollow circular disk, rotating with an angular acceleration under a changing temperature field, are achieved by applying a semi-analytical approach [4]. Dai examined a rotating circular disk with variable thickness under thermal environment [5]. Swaminathan investigated the effect of variation of material properties through the thickness, type of load case, boundary conditions, edge ratio, side-to-thickness ratio, and the effect of nonlinearity on the behavior of FGM plates [6]. Mohammad Zamani Nejad applied first-order shear deformation theory (FSDT) and multilayer method (MLM), a semi analytical solution has been performed for the purpose of elastic analysis of rotating thick truncated conical shells made of functionally graded materials (FGMs) under non-uniform pressure [7]. Guannan Wang employed a multi-scale model that investigate arbitrarily functionally graded hollow cylinders, with fibers, subjected to harmonic loading conditions [8]. Anh et al., research explored nonlinear stability analysis of thin annular spherical shells made of functionally graded materials on elastic foundations under external pressure and temperature [9]. Hosseini inspected the analysis of rotating nano-disk made of functionally graded materials with nonlinearly varying thickness based on strain gradient theory. Results indicate that compared to graded index, the effects of thickness parameters are greater the gap between the stress predicted by the classical theory, and the strain gradient theory is reported to be large only when the thickness of nano-disk is small [10]. Khanna inquired the analyses of steady state creep stresses and strain rates in a variable thickness rotating FGM disk that yields in agreement to Tresca criterion. The results are compared with those estimated applying the Von-Mises criterion [11]. Sahni an analytical solution in closed form is developed to computed stresses (radial and circumferential) made of functionally graded materials subjected to variable thickness and external pressure [12]. Farahmand explored the effect of autofrettage process parameters on the ultimate pressure that functionally graded spherical vessels can tolerate are investigated [13]. Afshin inspected a transient thermo-elastic analysis of a rotating thick cylindrical pressure vessel made of functionally graded material (FGM) subjected to axisymmetric mechanical and transient thermal loads [14]. Gharibi surveyed to find a way that *stresses* analysis of the functionally graded rotating thick cylindrical pressure vessels (FGRTCPV) [15]. Manthena contemplated Thermal stress analysis of a

thermosensitive functionally graded rectangular plate as a result of thermally induced resultant moments. The results indicate that the thermosensitive thermoelastic properties make notable effects on the transient temperature distribution [16]. Manthena and Kedar considered Transient thermal stress analysis of a functionally graded thick hollow cylinder with temperature-dependent material properties. The nature of temperature distribution and all stresses is reported to be sinusoidal when plotted for radial direction for both homogeneous and nonhomogeneous cases, and the magnitude of temperature distribution and all stresses was low for the nonhomogeneous case as compared to that of homogeneous case [17]. Manthena contemplated Effects of Stress Resultants on Thermal Stresses in a Functionally Graded Rectangular Plate as a result of Temperature Dependent Material Properties [18]. Lamba attempted to compute the temperature displacement function and stress functions due to partially distributed heat in a hollow cylinder. The governing heat conduction equation has been solved by applying Marchi-Zgrablich and Fourier sine transform techniques. The results are acquired in a series form in terms of Bessel's functions. A mathematical model has been constructed for the Aluminum material with the help of a numerical illustration [19]. Bousahlah attempted On thermal stability of plates with functionally graded coefficient of thermal expansion that in this article, a four-variable refined plate theory is presented for buckling analysis of functionally graded plates subjected to uniform, linear and non-linear temperature rises across the thickness direction. Equilibrium and stability equations are derived based on the present theory. The influences of many plate parameters on buckling temperature differences such ratio of thermal expansion, aspect ratio, side-to-thickness ratio, and gradient index have been inspected [20]. Bouderba contemplated thermal stability of functionally graded sandwich plates applying a simple shear deformation theory and results validated for a variety of numerical examples of the thermal buckling response of functionally graded sandwich plates with various boundary conditions [21]. Beldjelili attempted on Hygro-thermo-mechanical bending of S-FGM plates resting on variable elastic foundations using a four-variable trigonometric plate theory. The hygro-thermo-mechanical bending behavior of sigmoid functionally graded material (S-FGM) plate resting on variable two-parameter elastic foundations is discussed applying a four-variable refined plate theory [22]. El-Haina considered a simple analytical approach for thermal buckling of thick functionally graded sandwich plates. The purpose of this study was to present a simple

analytical approach in order to investigate the thermal buckling behavior of thick functionally graded sandwich by employing both the sinusoidal shear deformation theory and stress function. The thermal loads are contemplated as uniform, linear and non-linear temperature rises across the thickness direction. Numerical examples are presented to prove the effect of power law index, loading type and functionally graded layers' thickness on the thermal buckling response of thick functionally graded sandwich [23]. Menasria deliberated a new and simple HSDT for thermal stability analysis of FG sandwich plates. The novelty of this work is the application of a new displacement field that includes undetermined integral terms for analyzing thermal buckling response of functionally graded (FG) sandwich plates [24]. Bouderba considered Thermomechanical bending response of FGM thick plates resting on Winkler-Pasternak elastic foundations. He concluded that the proposed theory is accurate and efficient in predicting the thermomechanical bending response of functionally graded plates [25]. Hamidi reviewed a sinusoidal plate theory with 5-unknowns and stretching effects for thermomechanical bending of functionally graded sandwich plates. In this research, a simple yet accurate sinusoidal plate theory for the thermomechanical bending analysis of functionally graded sandwich plates is presented. Moreover, the effect of side-to-thickness ratio, aspect ratio, the volume fraction exponent, and the loading conditions on the thermomechanical response of functionally graded sandwich plates is investigated and discussed [26] as well. Mouffoki pondered Vibration analysis of nonlocal advanced nanobeams in hygro-thermal environment using a new two-unknown trigonometric shear deformation beam theory. In this work, the effects of moisture and temperature on free vibration characteristics of functionally graded (FG) nanobeams resting on the elastic foundation are examined by proposing a novel simple trigonometric shear deformation theory [27]. Tounsi contemplated a refined trigonometric shear deformation theory for thermoelastic bending of functionally graded sandwich plates. A refined trigonometric shear deformation theory (RTSDT) taking into account transverse shear. It can be concluded that the proposed theory is accurate and simple in solving the thermoelastic bending behavior of functionally graded plates [28]. Zidi considered bending analysis of FGM plates under hygro-thermo-mechanical. The bending response of functionally graded material (FGM) plate resting on elastic foundation and subjected to hygro-thermo-mechanical loading is studied loading using a four variable refined plate theory. The elastic foundation is modelled as two

parameter Pasternak foundation. Numerical results are given to verify the accuracy of present theory and the influences played by many parameters are explored [29].

In this study, four methods, variable material properties (VMP), Galerkin, Runge-Kutta with two different rules calculate the amount of displacement, stress, and strain of an FGM rotating disk in gas turbine engine.

2. General Assumptions Governing the Rotating Disk

The following assumptions are considered in order to simplify the equations and understanding the problem of modelling in a proper manner. Stress is not changed along with the thickness. The thickness of the disk varies from axis to blades and changes as the function of radius. The temperature varies as the specified function of the disk radius. Geometry, property distribution, and disk loading are axial symmetry. The disk rotates with a constant angular velocity. The compressive load of the shaft and centrifugal force applied in order to the blades are applied to the inner and outer surfaces of the disk as axial symmetry. The elasticity equations are presented based on the small strains in Eq. (1).

$$\varepsilon_r = \frac{du}{dr}, \ \varepsilon_\theta = \frac{u}{r}, \ \varepsilon = \varepsilon^e + \varepsilon^T \tag{1}$$

ρ is the disk density and term ε^T represents the thermal strain caused by the thermal gradient and εe the elastic strain caused by other loadings. The radial- peripheral stress-strain equations in the elastic state are presented in Eq. (2) and (3):

$$\varepsilon_r - \alpha\Delta T = \frac{1}{E}(\sigma_r - v\sigma_\theta) \tag{2}$$

$$\varepsilon_\theta - \alpha\Delta T = \frac{1}{E}(\sigma_\theta - v\sigma_r) \tag{3}$$

E is the modulus of elasticity, and v is the Poisson ratio, and α is the thermal expansion coefficient. The disk equilibrium equation is acquired by simplifying the forces applied to the disk in the form of Eq. (4):

$$\frac{d}{dr}(hr\sigma_r) - h\sigma_\theta + h\rho r^2\omega^2 = 0 \tag{4}$$

By substituting strain-displacement relations in strain-strain equations and substituting the resulting equation in the disk equilibrium Eq. (5) is obtained. This is a general equation of equilibrium of a disk with variable thickness and properties that are symmetric under the centrifugal and thermal load.

$$rhE\frac{d^2u}{dr^2} + \left(rh\frac{dE}{dr} + rE\frac{dh}{dr} + hE\right)\frac{du}{dr} \tag{5}$$

$$+\left(vE\frac{dh}{dr} + vh\frac{dE}{dr} - \frac{1}{r}Eh\right)u$$
$$+ (1-v^2)h\rho\omega^2 r^2$$
$$- r(1+v)\frac{d(hE\alpha\Delta T)}{dr} = 0$$

3. Problem Geometry

3.1. Boundary conditions

This condition is applied when there is no tension on the inner and outer surface of the disk.

$$@ \ r = r_i \ ; \ \sigma_r = 0$$
$$@ \ r = r_0 \ ; \ \sigma_r = 0 \tag{6}$$

This condition is utilized when compressive pressure p_{im} is applied on the inner surface of the disk and pm tension stress on the outer surface of the disk.

$$@ \ r = r_i \ ; \sigma_r = -p_{im}$$
$$@ \ r = r_0 \ ; \ \sigma_r = p_{im} \tag{7}$$

3.2. Properties distribution model

In order to deliberate the FGM material for the disk, a function must be contemplated, so the disk properties change from the inside-to-outside radius under that function. One of the best predictions for the properties distribution model is the power model applied in Eq. (8).

$$P(r) = (P_o - P_i)\left(\frac{r - r_i}{r_o - r_i}\right)^n + P_i; \ r_i < r < r_o \tag{8}$$

The disk thickness is a nonlinear variable which is obtained using Eq. (9).

$$h(r) = h_0\left(1 - q\left(\frac{r}{r_0}\right)^{m_1}\right) \tag{9}$$

4. The Methods used to Solve the Problem

Various analytical and numerical methods are used to confirm the results of this study. By applying multiple methods other than examining methods that are not used to solve these problems, we can compute the strengths and weaknesses and also it can be used for any kind of these problems.

4.1. VMP method

The VMP method is a semi analytical finite element method for solving differential equations that do not have an exact solution. In order to apply this method, the disk should be divided into loops with the same thickness, so that they have the same boundary condition of the forces on the common boundary. We must make the matrix Eq. (10) for each loop:

$$\begin{bmatrix} c_{11} & c_{12} \\ c_{21} & c_{22} \end{bmatrix}^{-1}\begin{Bmatrix} u_1 \\ u_2 \end{Bmatrix} = \begin{Bmatrix} \frac{F_1}{h} \\ \frac{F_2}{h} \end{Bmatrix} +$$
$$\begin{bmatrix} c_{11} & c_{12} \\ c_{21} & c_{22} \end{bmatrix}^{-1}\begin{Bmatrix} \Omega_1 \\ \Omega_2 \end{Bmatrix} + \begin{bmatrix} c_{11} & c_{12} \\ c_{21} & c_{22} \end{bmatrix}^{-1}\begin{Bmatrix} \theta_1 \\ \theta_2 \end{Bmatrix} \tag{10}$$

The coefficients are defined according to Eq. (11):

$$c_{11} = \frac{r_1}{E(r_2^2 - r_1^2)} \times$$
$$[(1 - v)r_1^2 + (1 + v)r_2^2]$$
$$c_{12} = \frac{2r_1 r_2^2}{E(r_1^2 - r_2^2)}$$
$$c_{21} = \frac{2r_1^2 r_2}{E(r_2^2 - r_1^2)}$$
$$c_{22} = \frac{r_2}{E(r_1^2 - r_2^2)} \times [(1 + v)r_1^2 + (1 - v)r_2^2] \tag{11}$$

$$\theta_1 = 2Ir_1$$
$$\theta_2 = (1 + v)r_2 J(r_2) + Ir_2[(1 - v) + (1 + v)\frac{r_1^2}{r_2^2}]$$

$$\Omega_1 = \frac{\rho\omega^2 r_1}{8E}[6r_2^2 + 2r_1^2 + 2vr_2^2 - 2vr_1^2]$$
$$\Omega_2 = \frac{\rho\omega^2 r_2}{8E}[2r_2^2 + 6r_1^2 - 2vr_2^2 + 2vr_1^2]$$

I and J are the functions of the Taylor expansion, and except for the radius at the beginning and end of each loop, the rest of the properties must be acquired at the mean radius of each loop. By solving the matrix Eq. (10), the displacement and force values are obtained for each node. Consequently, Eqs. (12) to (15) are applied in order r_0 acquire stress values.

$$\sigma_r = \left[A_1 - \frac{A_2}{r^2}\right] + \frac{3 + v}{8}\rho\omega^2\begin{bmatrix} r_2^2 + r_1^2 \\ \frac{r_1^2 r_2^2}{r^2} - r^2 \end{bmatrix} \tag{12}$$
$$+ E\left[-J(r) + I(1 - \frac{r_1^2}{r_2^2})\right]$$

$$\sigma_\theta = \left[A_1 + \frac{A_2}{r^2}\right] + \frac{3 + v}{8}\rho\omega^2\left[r_2^2 + r_1^2 \right.$$
$$+ \frac{r_1^2 r_2^2}{r^2} - \frac{1 + 3v}{3 + v}r^2\right]$$
$$+ E\left[J(r) - \alpha T(r) + I(1 + \frac{r_1^2}{r_2^2})\right] \tag{13}$$

$$A_1 = \frac{F_2 r_2^2 - F_1 r_1^2}{(r_1^2 - r_2^2)h}, A_2 = \frac{(F_2 - F_1)r_1^2 r_2^2}{(r_1^2 - r_2^2)h} \tag{14}$$

$$T(r) = A \ln\left(\frac{r}{r_0}\right) + T_0$$
$$A = \frac{T_i - T_0}{\ln\frac{r_i}{r_0}} \tag{15}$$

4.2. Galerkin method

The Galerkin method is a finite element solving method which is beneficial in the process of solving the differential equation governing the rotating FGM disk by elementalizing the disk. The hardness matrix and force of each element and total force can be acquired by integrating the shape functions and the equation governing the element volume and adding the boundary conditions to the governing equation and combining them. Various elements can be applied in the Galerkin method, which the Hermitian element has been used in this study. The Hermitian element uses four shape functions, and to calculate the value of displacement derivative, the element is taken from the derivative of the two shape functions in two points. Due to the application of four shape functions, the displacement derivatives, the more precise answers can be obtained, especially in nodes. Considering the Eq. (5) and the simplification of the coefficients using letters, the equation governing disk is obtained in the form of Eq. (16).

$$Au'' + Bu' + Cu + D = 0 \tag{16}$$

After solving the problem using the Galerkin method, first, the Lagrangian element is described with two shape functions, and finally, the changes are made that must be applied to the equations for the Hermitian element. The displacement is defined by equation (17):

$$u = N_i u_i + N_j u_j \tag{17}$$

N_i and N_j are shape functions in a linear mode that is defined as follows (18):

$$N_i = \frac{r_j - r}{l}, N_j = \frac{r - r_i}{l} \tag{18}$$

r_j is the coordinate of the end point, r_i is the initial coordinates, and l is the element length.

Then, the Galerkin method is applied to Eq. (16) and Eq. (19) and (20) is obtained. Eq. (23) and (22) are obtained by simplifying the integral (20):

$$\int N_i(Au'' + Bu' + Cu + D)dv = 0$$
$$\int N_j(Au'' + Bu' + Cu + D)dv = 0 \tag{19}$$

$$dv = rdrd\theta dz \tag{20}$$

$$\int_0^{2\pi} \int_{-\frac{h}{2}}^{\frac{h}{2}} \int_{r_i}^{r_o} N(Au'' + Bu' + Cu \\ + D)rdrdzd\theta = 0 \tag{21}$$

$$\int N_i(Au'' + Bu' + Cu + D)2\pi rdrh = 0 \tag{22}$$
$$\int N_j(Au'' + Bu' + Cu + D)2\pi rdrh = 0$$

The first relation of Eq. (22) is solved by the method by parts and Eq. (23) and (24) are obtained.

$$(rN_iA)hu'\big|_{ri}^{ro} - \int (rN_iAh)'u'dr + \\ \int rN_ih(Bu' + Cu + D)dr = 0 \tag{23}$$

$$(rN_jA)hu'\big|_{ri}^{ro} - \int (rN_jAh)'u'dr + \\ \int rN_jh(Bu' + Cu + D)dr = 0 \tag{24}$$

u' is the derivative of the displacement relative to the radius, which is obtained from Eq. (25):

$$\sigma_r = \frac{E}{(1-v^2)}\left(\frac{du}{dr} + v\frac{u}{r} - (1+v)\alpha\Delta T\right) \\ \sigma_\theta = \frac{E}{(1-v^2)}\left(v\frac{du}{dr} + \frac{u}{r} - (1+v)\alpha\Delta T\right) \tag{25}$$

By expanding the Eq. (22), we obtain Eq. (26) to (27).

In the following, applying the Eq. (28) and (29), the stiffness and force matrices of each element are obtained as equation (30):

$$\left[\int\int (-(rN_iAh)'{}^{N_i'} + rN_ihBN_i' \\ + rChN_iN_i)dr\right]u_i \\ + \left[\int\int (-(rN_iAh)'N_j' \\ + rN_ihBN_j' \\ + rChN_iN_j)dr\right]u_j \\ + \int rN_ihDdr = 0 \tag{26}$$

$$\left[\int\int [-(rN_iAh)'N_i' + rN_ihBN_i' \\ + rChN_iN_i)dr\right]u_i \\ + \left[\int\int (-(rN_jAh)'N_j' \\ + rN_jhBN_j' \\ + rChN_jN_j)dr\right]u_j \\ + \int rN_jhDdr = 0 \tag{27}$$

At last, the total stiffness matrix of the structure is computed as

$$k_{ii}u_i + k_{ij}u_j = f_i$$
$$k_{ji}u_i + k_{jj}u_j = f_j \tag{28}$$
$$[K_{ele\,u}]_{2\times2}[u_{ele\,u}]_{2\times1} = [f_{ele\,u}]_{2\times1}$$

where, N is the number of loops. Consequently, using Eq. (31) and having values of the hardness

and force matrices, the total displacement values in each node are obtained:

$$[K_T][u_T] = [f_T] \qquad (29)$$

4.3. Hermitian element

The governing equations and solving process of Galerkin Hermitian type are similar to the two-degree freedom mode. In this case the difference can be explained as four shape functions been applied, and their relationships and the Jacobi related to convert the disk radius -dependent variable is discussed below. The relationship between displacement and four shape functions of the Hermitian element is presented in Eq. (30).

$$u^e = N_1 u_1 + N_2 \frac{du}{d\xi}\Big|1 + N_3 u_2 + N_4 \frac{du}{d\xi}\Big|2 \qquad (30)$$

where, $\frac{du}{d\xi}$ is the derivative of the displacement relative to the location at the beginning and end of each element. The relations of the shape functions are given in Eq. (31). Where ξ is equivalent to a radius in the local coordinates of each element.

$$N_1 = \frac{1}{4}(\xi^3 - 3\xi + 2)$$

$$N_2 = \frac{1}{4}(\xi^3 - \xi^2 - \xi + 1)$$

$$N_3 = -\frac{1}{4}(\xi^3 - 3\xi - 2) \qquad (31)$$

$$N_4 = \frac{1}{4}(\xi^3 + \xi^2 - \xi - 1)$$

Applying a Cubic equation, three shape functions with a continuous definition space and in the form of a third-order curve from the distribution of values of the shape functions in each element can be acquired. The Jacobi equation with the length of each element in the Hermitian method is presented by (32) and (33):

$$[J] = \frac{L}{2}$$

$$dr = \frac{L}{2} \times d\xi \qquad (32)$$

$$r = N_1 r_1 + N_2 \frac{dr}{d\xi}\Big|1 + N_3 r_2 + N_4 \frac{dr}{d\xi}\Big|2$$

$$L = r_2 - r_1$$

By expanding the integral of the shape functions and the differential equation governing the values of the stiffness matrix elements and force of each element, and by solving the matrix equation, the values of displacement, the stress and strain are obtained respectively.

4.4. Runge–Kutta method

ψ is stress function, and stress-strain relations are defined as (33). Runge–Kutta, with the elementalization of the problem and guessing an initial value for ψ', and the transfer of the values

of ψ and ψ' from the inner surface node from each node to the next node in step form, and eventually reaching to ψ and ψ' of the node, the outer surface of the disk, the values of displacement, stress and strain are achieved in the nodes of each element. This trend can be the opposite and to be from the outside toward the inside as well. If the ψ obtained at the last node is the same boundary condition of the problem, the process is correct, however if there is a difference, consequently the initial guess must be corrected ψ', and the same process must be continued.

$$\sigma_r = \frac{1}{hr}\psi$$

$$\sigma_\theta = \frac{1}{h}\frac{d\psi}{dr} + \rho\omega^2 r^2$$

$$\varepsilon_r - \alpha\Delta T = \frac{1}{E}(\sigma_r - v\sigma_\theta) \qquad (33)$$

$$\varepsilon_\theta - \alpha\Delta T = \frac{1}{E}(\sigma_\theta - v\sigma_r)$$

$$\frac{d}{dr}(r\varepsilon_\theta) - \varepsilon_r = 0$$

The order of differential equations governing the disk decreases to one by changing the variable and contemplating two first-order equations simultaneously, Eq. (34) is acquired:

$$z' + \frac{B}{A}z + \frac{C}{A}\psi + \frac{D}{A} = 0$$

$$z' = -\frac{B}{A}z - \frac{C}{A}\psi - \frac{D}{A} \qquad (34)$$

$$z = \psi'$$

By placing the strain-displacement relations in the equilibrium Eq. (4), the relation of the disk elastic region equilibrium is obtained in the form of Eq. (35), which all derivatives are in terms of r. Boundary conditions are determined by Eq. (36); these values are set to a value instead of zero when the compressive effect of the shaft and centrifugal of the blades is considered. Due to the application of the Taylor Four-Order term, the most accurate results are acquired by Four-Order Runge–Kutta. The two common types of Runge–Kutta is Simpson 1/3 and Simpson 3/8. Using Eq. (38), the Simpson1/3 equation is defined.

$$\begin{Bmatrix} z' \\ \psi' \end{Bmatrix} = \left\{ \underset{z}{-\frac{B}{A}z - \frac{C}{A}\psi - \frac{D}{A}} \right\} = F(r, z, \psi)$$

$$X = \begin{Bmatrix} z' \\ \psi' \end{Bmatrix} \qquad (35)$$

$$\left\{ \underset{z}{-\frac{B}{A}z - \frac{C}{A}\psi - \frac{D}{A}} \right\} = F(r, z, \psi)$$

$$r^2\psi'' = -\left(1 - r\frac{h'}{h} - r\frac{E'}{E}\right)r\,\psi'$$
$$+\left(1 - vr\frac{h'}{h} - vr\frac{E'}{E}\right.$$
$$\left. + v'r\right)\psi - (3 + v - r\frac{E'}{E} \tag{36}$$

$$+ r\frac{\rho'}{\rho})hpw^2r^3 - Ehr^2(\alpha'\Delta T + \alpha\Delta T')$$

$$\sigma_r = 0 \quad ; \quad \psi = 0 \quad , \quad r = r_i$$
$$\sigma_r = 0 \quad ; \quad \psi = 0 \quad , \quad r = r_o \tag{37}$$

$$X = F(r, z, \psi)$$
$$X_{i+1} = X_i + \frac{1}{6}(k_1 + 2k_2 + 2k_3 + k_4)$$
$$k_1 = hf(r_i, X_i)$$
$$k_2 = hf(X_i + \frac{k_1}{2}, r_i + \frac{h}{2}) \tag{38}$$
$$k_3 = hf(X_i + \frac{k_2}{2}, r_i + \frac{h}{2})$$
$$k_4 = hf(X_i + k_3, r_{i+1})$$

h is the length of each element. The relationship related to the Simpson 3/8 rule is presented in Eq. (39).

$$X = F(r, z, \psi)$$
$$X_{i+1} = X_i + \frac{1}{8}(k_1 + 3k_2 + 3k_3 + k_4)$$
$$k_1 = hf(r_i, X_i)$$
$$k_2 = hf(X_i + \frac{k_1}{3}, r_i + \frac{h}{3}) \tag{39}$$
$$k_3 = hf(X_i - \frac{k_1}{3} + k_2, r_i + \frac{2h}{3})$$
$$k_4 = hf(X_i + k_1 - k_2 + k_3, r_{i+1})$$

In this study, two problems with dissimilar properties have been solved, and each problem is divided into two modes, including temperature-independent and temperature-dependent properties. The characteristics of these four modes are presented in Tables 1 and 2, respectively.

5. Results and Discussion

After the application of disk properties in each condition and for each input of the problem, the results of each method and each state were attained, and these are presented as diagrams.

5.1. The results of the first problem in the state of dis-relation of the properties on the temperature

Pursuant to the Fig. 1, whatever we move from the internal radius of the disk towards its end, the amount of displacement of the desired node increases, which it is as a result to the boost in the radius and the amount of centrifugal force and the reduction of this force reverse confronting in the large radius of disk.

Table 1 Disk properties of the first and the second problem in the state of independent properties of temperature.

Inner surface	Outer surface	properties
70×10^9	151×10^9	Elasticity Module (Pa)
0.3	0.3	Poisson Ratio
2700	5700	Density $(\mathrm{Kg/m^3})$
0	100	Temperature(°C) for the first problem
100	200	Temperature (°C) for the second problem
500	500	Angular speed (rad/sec) for the first problem
5670	5670	Angular speed (rad/sec) for the second problem
23×10^{-6}	10×10^{-6}	Thermal expansion coefficient (1/°C)
0.5	0.5	M
0.96	0.96	Q
0.02	0.02	h_0
0.1	0.5	r_1, r_2 (m) for the first problem
0.01	0.11	r_1, r_2 (m) for the second problem

Table2 Disk properties of the first problem in the state of dependent properties of temperature

Inner surface	Outer surface	Properties	
122.56×10^9	244.27×10^9	p_0	
0	0	p_{-1}	Elasticity Module (Pa)
-4.59×10^{-4}	-1.37×10^{-3}	p_1	
0	1.214×10^{-6}	p_2	
0	-3.68×10^{-10}	p_3	
0.3	0.3	Poisson Ratio	
4429	3000	Density $(\mathrm{Kg/m^3})$	
0	100	For the first problem Temperature(°C)	
100	200	For the second problem Temperature(°c)	
500	500	Angular speed (rad/sec)	
0.5	0.5	M	
0.96	0.96	Q	
0.02	0.02	h_0	
0.1	0.5	r_1, r_2 (m) for the first problem	
0.01	0.11	r_1, r_2 (m) for the second problem	
7.5788×10^{-6}	12.766×10^{-6}	p_0	
0	0	p_{-1}	Thermal expansion coefficient (1/°C)
6.638×10^{-4}	-1.49×10^{-3}	p_1	
-3.15×10^{-6}	1.006×10^{-5}	p_2	
0	-6.78×10^{-11}	p_3	

In consonance to Figs. 2 and 3, there is maximum radial stress in the central points of the disk and is zero at the beginning and end points because of the radial loading of the disk. The peripheral stress also has the highest value at the beginning and end of the disk and is minimized at a radius of 0.35. Fig. 2 indicates radial stress results by VMP and Galerkin and Runge-Kutta methods and Fig. 3 contemplates hoop stress by four methods that have similar results.

Confirming to Figs. 4 and 5, the radial strain of the disk, considering the radial directional load, starts at its lowest value and reaches its maximum value in the radius of 0.3 (m). The changes in peripheral strain are more uniformly and decrease with a slight gradient in the middle of the disk; however, this again increases at the end of the disk. Fig. 4 displays radial strain results by VMP and Galerkin and Runge-Kutta methods and Fig. 5 considers hoop strain by four methods that have similar results.

5.2. The results of the first problem in the state of dependence of the properties on the temperature

Pursuant to Fig. 6, it can be concluded that in the state of dependence of the properties on the temperature, the displacement variation interval decreased but numerical values are increased.

With respect to Figs. 7 and 8, the amounts of environmental stress and radial stress in the state of dependence of the properties on the temperature have increased, and the form of the variations of environmental stress diagram becomes completely descending.
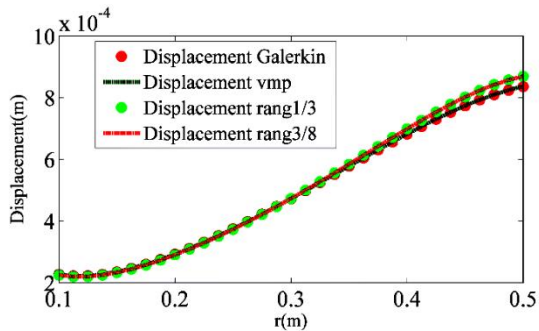
Fig. 1 Chart of displacement four methods of the first problem
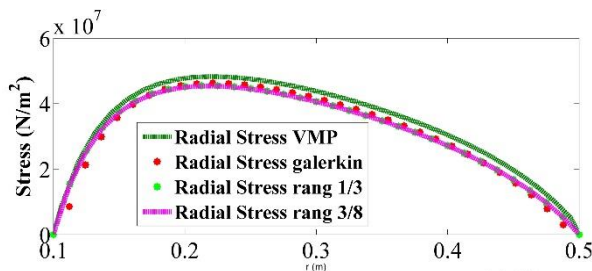
Fig. 2 Chart of radial stress by VMP and Galerkin and Runge Kutta methods of the first problem
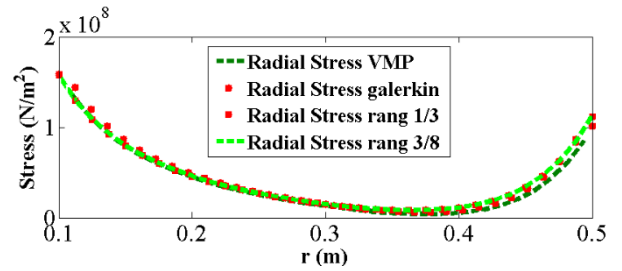
Fig. 3 Chart of hoop stress by VMP and Galerkin and Runge Kutta methods of the first problem
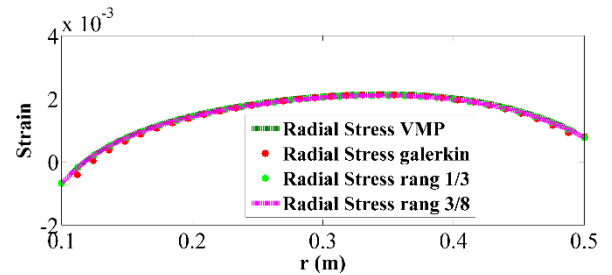
Fig. 4 Chart of radial strain by VMP and Galerkin and Runge Kutta methods of the first problem
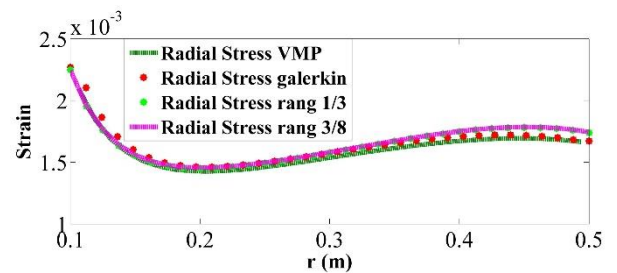
Fig. 5 Chart of hoop strain by VMP and Galerkin and Runge Kutta methods of the first problem
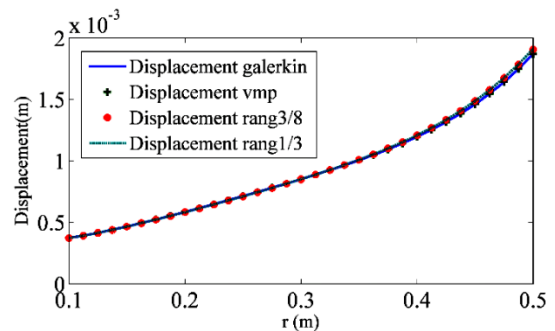
Fig. 6 Chart of displacement by four methods of the first problem
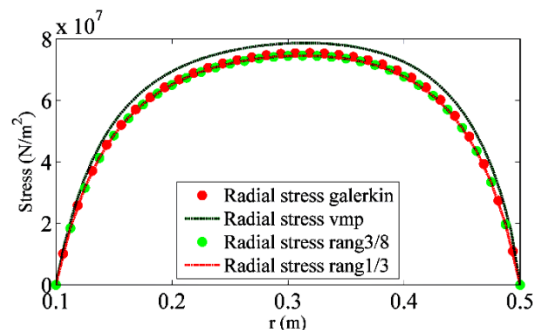
Fig. 7 Chart of radial stress by four methods of the first problem
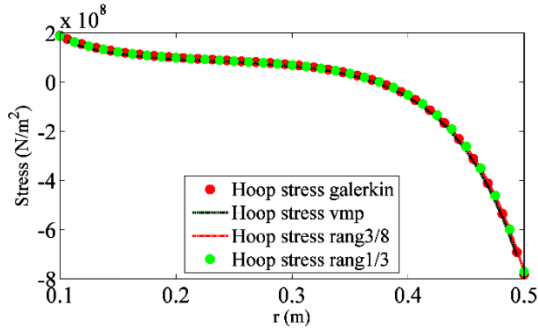
Fig. 8 Chart of hoop stress by four methods of the first problem

With respect to the Figs. 9 and 10, the form of variations of the radial strain in the state of dependence of the properties on the temperature becomes completely ascending, and numerical values are enhancing as well.

5.3. The results of the second problem in the state of dis-relation of the properties on the temperature and disregarding the boundary conditions

With respect to Fig. 11, the geometry of the disk is smaller in this problem, and the loadings have increased which is the reason for decreasing the displacement variation interval, but the form of the variations is as before.

With respect to the Figs. 12 and 13, the maximum of the radial stress in the radius of 0.03 (m) and the maximum of the environmental stress in the radius of 0.11 (m) have been achieved.
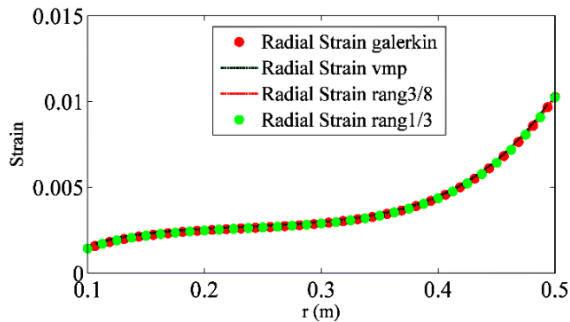
Fig. 9 Chart of radial strain by four methods of the first problem
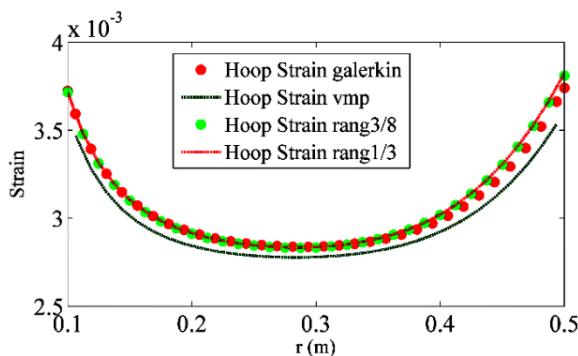
Fig. 10 Chart of hoop strain by four methods of the first problem
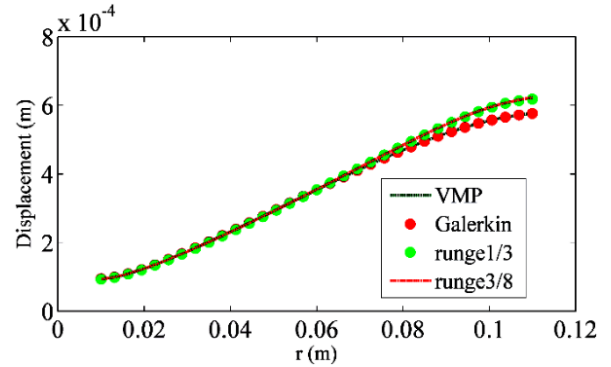
Fig. 11 Chart of displacement by four methods of the first mode and the second problem
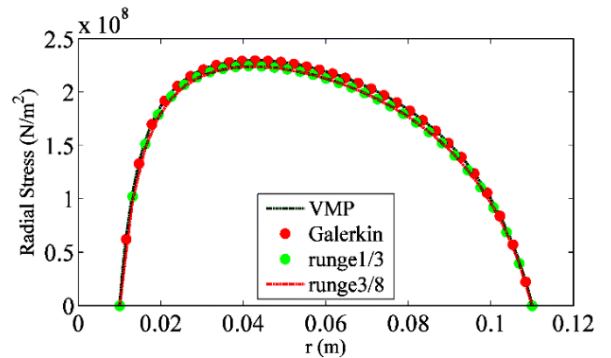
Fig. 12 Chart of radial stress by four methods of the first mode and the second problem
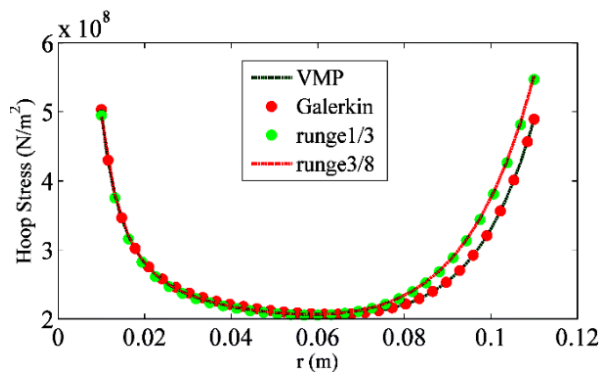
Fig. 13 Chart of hoop stress by four methods of the first mode and the second problem

According to the Figs. 14 and 15, the maximum of the radial strain in the radius of 0.05 (m) and the maximum of the environmental stress in the radius of 0.01(m) have been attained.

5.4. The results of the second problem in the state of dis-relation of the properties on the temperature and taking into account the boundary conditions

With respect to the Figs. 16 to 20, all the amounts of stress and strain with respect to the previous state have enhanced by adding boundary conditions. This can be explained as the radial loading. That Fig. 16 illustrates displacement, Fig. 17 indicates radial stress; Fig. 18 displays hoop stress, Fig. 19 shows radial strain and Fig. 20 portrayed hoop strain amounts by four methods.
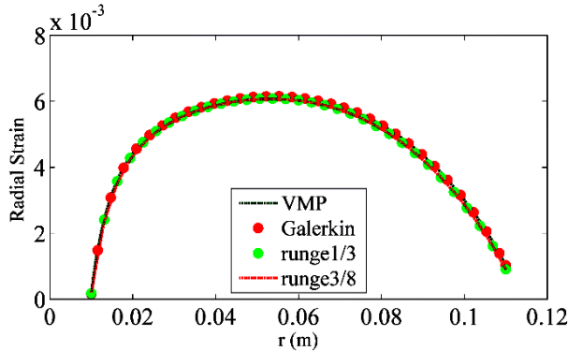
Fig. 14 Chart of radial strain by four methods of the first mode and the second problem
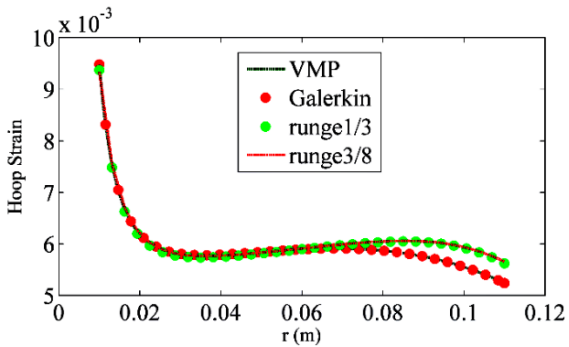
Fig. 15 Chart of hoop strain by four methods of the first mode and second problem
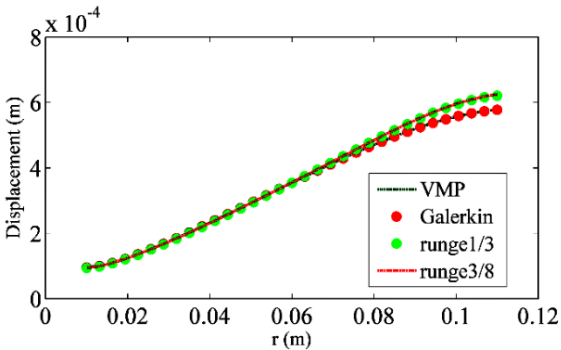
Fig. 16 Chart of displacement by four methods of the second mode and second problem
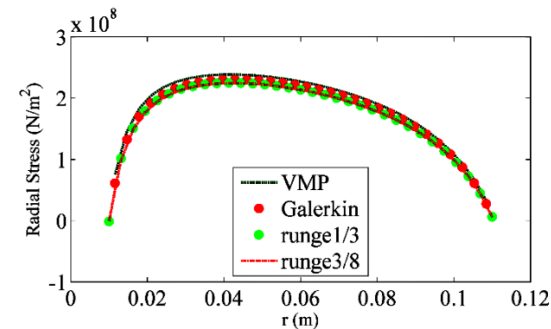
Fig. 17 Chart of radial stress by four methods of the second mode and second problem

5.5. The results of the second problem in the state of dependence of the properties on the temperature and disregarding the boundary conditions

Pursuant to Figs. 21 to 25, when the properties depend on the temperature, other than increasing of the stress followed by increasing of the strain of the environmental stress and radial strain, form of the variations become different from the state in which properties are independent of temperature, and they become completely descending and completely ascending respectively. That Fig. 21 indicates displacement, Fig. 22 reveals hoop strain, Fig. 23 displays radial strain, Fig. 24 shows radial stress, and Fig. 25 illustrates hoop stress amounts by four methods.
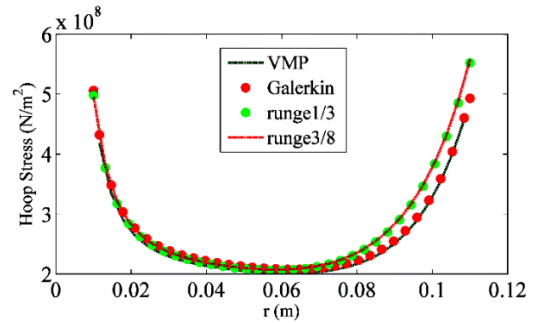
Fig. 18 Chart of hoop stress by four methods of the second mode and second problem
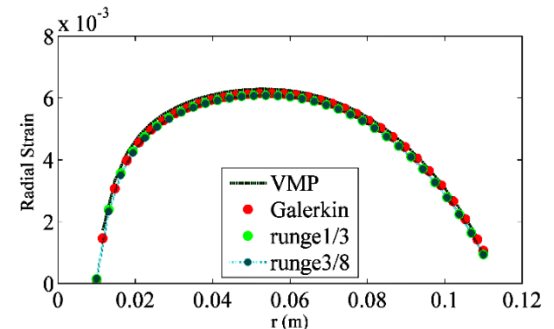
Fig. 19 Chart of radial strain by four methods of the second mode and second problem
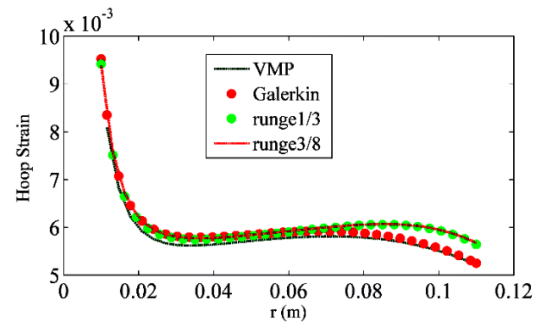
Fig. 20 Chart of hoop strain by four methods of the second mode and second problem
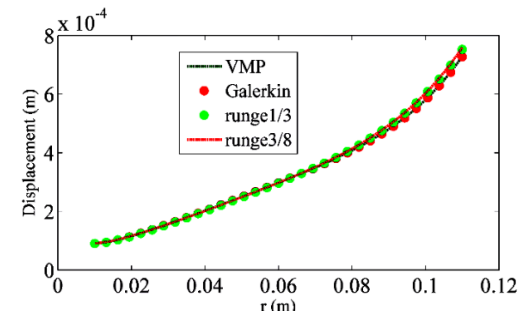
Fig. 21 Chart of displacement by four methods of the third mode and second problem
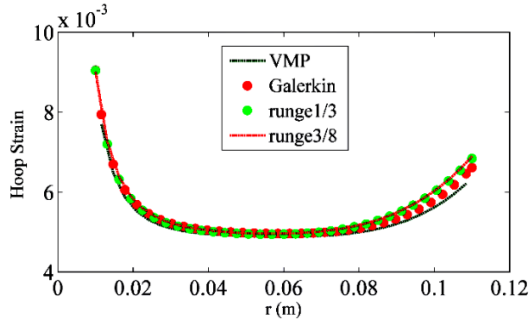
Fig. 22 Chart of hoop strain by four methods of the third mode and second problem
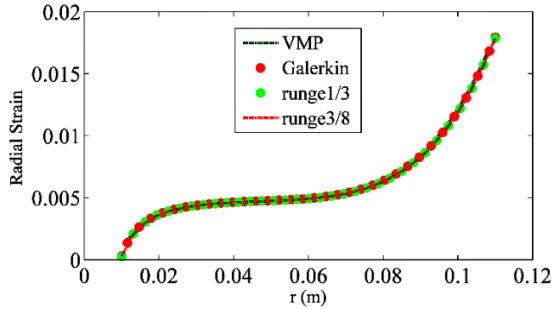
Fig.23 Chart of radial strain by four methods of the third mode and second problem
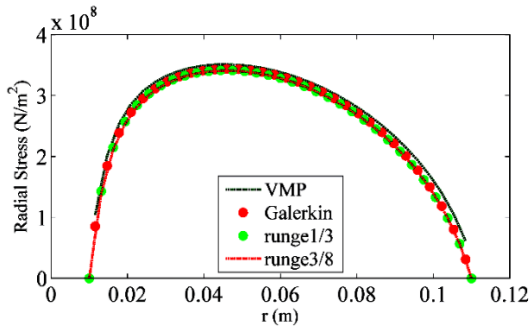
Fig.24 Chart of radial stress by four methods of the third mode and second problem
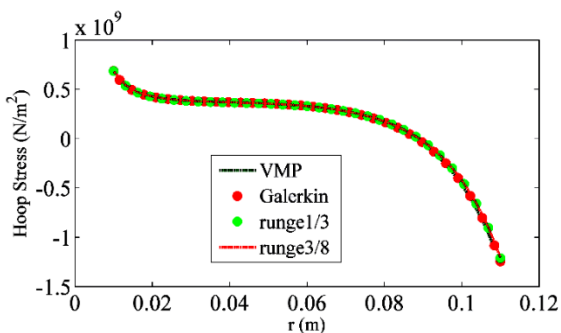
Fig. 25 Chart of hoop stress by four methods of the third mode and second problem

5.6. The results of the second problem in the state of dependence of the properties on the temperature and taking into account the boundary conditions

With respect to the Figs. 26 to 30, the amounts of stress and strain with respect to the previous state have enhances by adding boundary conditions. This can be explained as the radial

loading of the disk, although the amount of loading in the boundary conditions is small relative to the original loading and has a small impact on the diagrams as well as on the increasing of stresses. That Fig. 26 displays displacement, Fig. 27 indicates radial stress, Fig. 28 shows hoop stress, Fig. 29 shows radial strain and Fig. 30 illustrates hoop strain amounts by four methods.
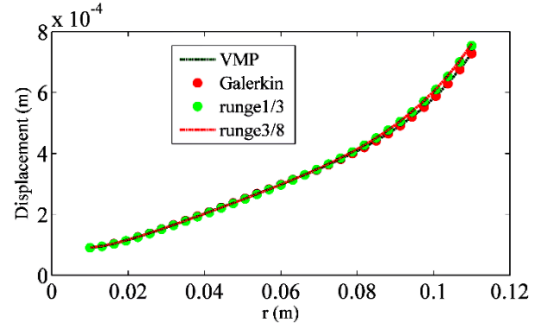
Fig. 26 Chart of displacement by four methods of the fourth mode and second problem
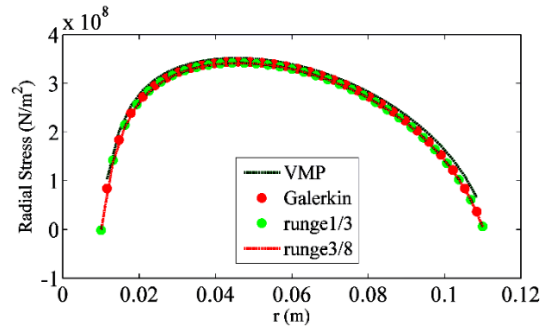
Fig. 27 Chart of radial stress by four methods of the fourth mode and second problem
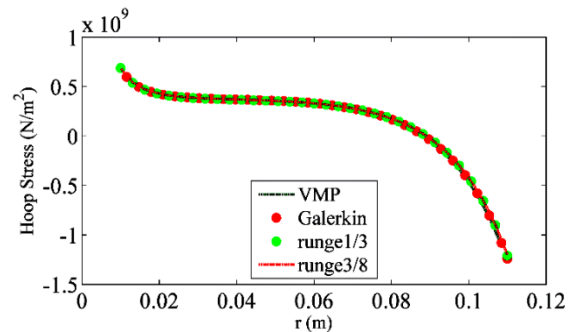
Fig. 28 Chart of hoop stress by four methods of the fourth mode and second problem
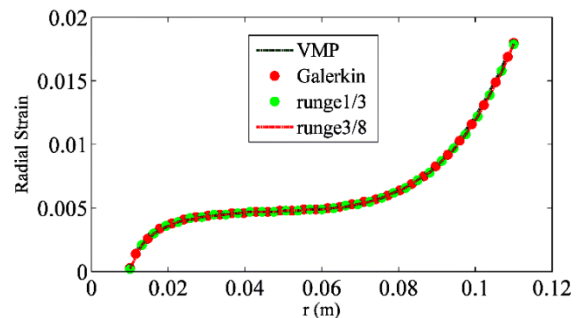
Fig. 29 Chart of radial strain by four methods of the fourth mode and second problem
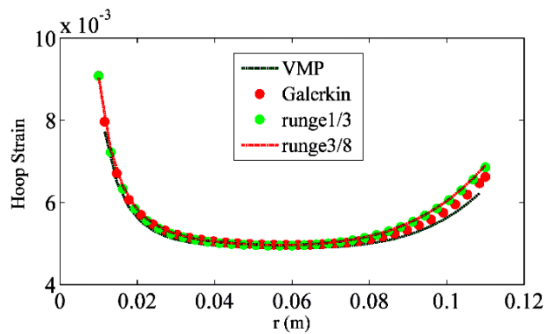
Fig. 30 Chart of hoop strain by four methods of the fourth mode and second problem

6. Conclusions

Overall in this paper, we deliberated two problems; each one of them had a different geometry and loading. It is concluded that the amount of stress and strain will increase with the decrease of disk dimensions as well as an increase in the amount of eccentricity force and temperature difference. The second problem was contemplated in four states and it is concluded that, when adding boundary conditions, as a result to the boost of radial loading, there is an increase in the amount of stress and strain, although it is not very much due to the small the amount of boundary loading relative to the original loading.

Solving the problem by dissimilar methods leads to validate of the results, and the capability of each method in this kind of problems was estimated. VMP method doesn't lead to any exact answer in nodes, because of the gain of stress and strain in the middle points of each element and discontinuity in the nodes. It is a drawback of this method, but we can compensate this drawback by increasing the number of elements. Runge–Kutta method is an iterative finite element method. The advantage of this method is exact solutions as a result of being exact the own boundary conditions of loading, and the drawback of the method is time-consuming. It can be said that the Galerkin method is so extensive and each state of this method can be applied the best to answer a family of problems. The Hermitian element method utilized in this paper continues in nodes owing to presence of derivative terms of displacement related to the location in the nodes. This method has the capability of computation of stress and strain in the middle of the element and in the nodes. The critical points of stress in most of the states are in the middle of the disk for radial stress and in the boundaries for environmental stress. At the equivalent stress, this also occurs in the initial and the final terminations of the disk.

Comparing two numerical computed problems (section 5.1 with 5.3) reducing disk size, lead to decreasing maximum displacement of 0.00083m to 0.00068 m, increasing the maximum radial stress value from 51 MPa to 240 MPa and increasing the maximum environmental stress from 160 MPa to 580 MPa. Also, values of radial and environmental strains increased from 0.0025 to 0.0065 and from 0.0023 to 0.0095, respectively.

Comparing the first problem with properties independent of temperature with properties dependence to temperature (results in sec. 5.1 and 5.2) shows that considering thermal effects i.e., the results of Section 5.1 in comparison with Section 5.2, cause increase in maximum displacement from 0.00083 to 0.0019 mm, in maximum radial stress from 51 to 79 MPa and in maximum environmental stress from 160 MPa to 210 MPa. Moreover, values of radial and environmental strains increased from 0.0025 to 0.012 and from 0.0023 to 0.0038 respectively.

Comparing the ideal loading condition for the second problem (Section 5.3) with the most critical condition of second problem (Section 5.6) shows that the maximum displacement increased from 0.00068 to 0.00078 mm, the maximum radial stress increased from 240 to 340 MPa, and the maximum environmental stress increased from 580 to 700 MPa. Also, values of radial and environmental strains increased and reduced from 0.0065 to 0.018 and from 0.0095 to 0.0093, respectively.

References

1. Sahni M, Sahni R. Rotating Functionally Graded Disc with Variable Thickness Profile and External Pressure. P*rocedia Computer Science* 2015; 57: 1249-1254.
2. Arnab B. Finite difference solution to thermoelastic field in a thin circular FGM disk with a concentric hole. *Procedia Engineering* 2014; 90: 193-198.
3. Bayat M. One-dimensional analysis for magneto-thermo-mechanical response in a functionally graded annular variable-thickness rotating disk. *Applied Mathematical Modelling* 2014; 38(19-20): 4625-4639.
4. Dai T, Dai H. Thermo-elastic analysis of a functionally graded rotating hollow circular disk with variable thickness and angular speed. *Applied Mathematical Modelling* 2016; 40(17-18): 7689-7707.
5. Dai T, Dai H. Analysis of a rotating FGMEE circular disk with variable thickness under thermal environment. *Applied Mathematical Modelling* 2017; 45: 900-924.
6. Swaminathan K. Stress, vibration and buckling analyses of FGM plates—A state-of-the-art review. *Composite Structures* 2015; 120: 10-31.

7. Nejad M.Z., Jabbari M, Ghannad M. Elastic analysis of FGM rotating thick truncated conical shells with axially-varying properties under non-uniform pressure loading. *Composite Structures* 2015; 122: 561-569.

8. Wang G, Dong L, Atluri S.N. Direct and Inverse Multi-Scale Analyses of Arbitrarily Functionally Graded Layered Hollow Cylinders (Discs), with Different Shaped Reinforcements, under Harmonic Loads. *Composite Structures*, 2018.

9. Anh, V.T.T., Bich D.H., Duc N.D. Nonlinear stability analysis of thin FGM annular spherical shells on elastic foundations under external pressure and thermal loads. *European Journal of Mechanics-A/Solids* 2015; 50: 28-38.

10. Hosseini M. Stress analysis of rotating nano-disks of variable thickness made of functionally graded materials. *International Journal of Engineering Science* 2016; 109: 29-53.

11. Khanna K, Gupta V, Nigam S. Creep analysis in functionally graded rotating disc using tresca criterion and comparison with von-mises criterion. *Materials Today: Proceedings* 2017; 4(2): 2431-2438.

12. Sahni M, Sahni R, Mehta P. Creep Behaviour under SiCp Exponential Volume Reinforcement in FGM Composite Rotating Cylinders. *Materials Today: Proceedings* 2017; 4(9): 9529-9533.

13. Farahmand S, Atai A. Parametric investigation of auto-frettage process in thick spherical vessel made of functionally graded materials. *Journal of Computational Applied Mechanics* 2016; 47(1): 9.

14. Afshin A, Zamani Nejad M, Dastani K. Transient thermoelastic analysis of FGM rotating thick cylindrical pressure vessels under arbitrary boundary and initial conditions. *Journal of Computational Applied Mechanics* 2017; 48(1): 15-26.

15. Gharibi M, Nejad M.Z, Hadi A. Elastic analysis of functionally graded rotating thick cylindrical pressure vessels with exponentially-varying properties using power series method of Frobenius. *Journal of Computational Applied Mechanics* 2017; 48(1): 89-98.

16. V.R. Manthena. Thermal stress analysis of a thermosensitive functionally graded rectangular plate due to thermally induced resultant moments. *Multidiscipline Modeling in Materials and Structures* 2018.

17. V.R. Manthena, Kedar G.D. Transient thermal stress analysis of a functionally graded thick hollow cylinder with temperature- dependent material properties, *Journal of Thermal Stresses* 2018; 41(5): 568-582.

18. V.R. Manthena. Effects of stress resultants on thermal stresses in a functionally graded rectangular plate due to temperature dependent material properties, *International Journal of Thermodynamics* 2018; 19(4); 235-242.

19. N. K. Lamba. Stress functions in a hollow cylinder under heating and cooling Process. *Journal of Statistics and Mathematics* 2018; 3 (3): 118-124.

20. Bousahla. On thermal stability of plates with functionally graded coefficient of thermal expansion. *Struct. Eng. Mech* 2016; 60(2): 313-335.

21. Bouderba. Thermal stability of functionally graded sandwich plates using a simple shear deformation theory. *Struct. Eng. Mech* 2016; 58(3): 397-422.

22. Beldjelili. Hygro-thermo-mechanical bending of S-FGM plates resting on variable elastic foundations using a four-variable trigonometric plate theory. *Smart Structures and Systems* 2016; 18(4): 755-786.

23. El-Haina. A simple analytical approach for thermal buckling of thick functionally graded sandwich plates. *Struct. Eng. Mech* 2017; 63(5): 585-595.

24. Menasria. A new and simple HSDT for thermal stability analysis of FG sandwich plates. *Steel and Composite Structures* 2017; 25(2): 157-175.

25. Ouderba. Thermomechanical bending response of FGM thick plates resting on Winkler–Pasternak elastic foundations. *Steel and Composite Structures* 2013; 14(1): 85 – 104.

26. Hamidi. A sinusoidal plate theory with 5-unknowns and stretching effect for thermomechanical bending of functionally graded sandwich plates. *Steel and Composite Structures* 2015; 18(1): 235 – 253.

27. Mouffoki. Vibration analysis of nonlocal advanced nanobeams in hygro-thermal environment using a new two-unknown trigonometric shear deformation beam theory. *Smart Structures Systems* 2017; 20(3): 369-383.

28. Tounsi. A refined trigonometric shear deformation theory for thermoelastic bending of functionally graded sandwich plates. *Aerosp. Sci. Technol* 2013; 24(1): 209-220.

29. Zidi. Bending analysis of FGM plates under hygro-thermo-mechanical loading using a four variable refined plate theory. *Aerospace Sci* 2014; 24-34.

.